# Exploring Effect of Microproperties on Shear Strength of Rock Joints through Physical and Numerical Modeling

Hoang-Khanh Le[1]; Wen-Chao Huang[2]; Meng-Chia Weng, M.ASCE[3]; and Wen-Jeng Huang[4]

**Abstract:** Understanding the shear strength and failure mechanism of a rock joint is essential in rock engineering. This study performed a series of direct shear tests and discrete element modelings on artificial joint specimens to investigate the effect of roughness [randomly generated joint profiles with joint roughness coefficient (JRC) = 20, 19.6, and 10] on the joint strength. The results of the numerical simulation were consistent in the peak shear strength with the laboratory tests and Barton's equation. From a microscopic viewpoint, the rock joint's peak and residual shear strength were mainly mobilized from the friction property of such a joint profile. The contribution of friction to the shear strength at the residual stage was reduced because of dilation behavior and decreasing contact area along the joint surface. Therefore, the mobilized friction angle decreased from the initial basic friction angle to a certain value depending on the initial JRC value. The mobilized JRC of a rock joint was found to be related to the initial JRC, the unconfined compressive strength (UCS) of joint material, and the applying normal stress. The surface of joint models with high UCS is less damaged than that with low UCS. Finally, a new model for predicting the residual shear strength of a rock joint was also proposed, which can be applied for the joint using both randomly generated profiles and Barton's standard profiles. **DOI: 10.1061/(ASCE)GM.1943-5622.0002432**. 

**Author keywords:** Artificial rock joints; Discrete element method model; Peak and residual shear strength; Mobilized joint roughness coefficient; Mobilized friction angle.



## Introduction

The mechanical behavior of fractures strongly influences the peak and residual shear strength of rock mass, which needs to be estimated to design underground structures, rock slope, and tunneling. Barton (1973) performed a series of direct shear (DS) tests on jointed rock specimens. The test results indicated that the peak shear strength was highly related to the normal stress, the joint roughness coefficient (JRC), and the unconfined compressive strength (UCS) of such a joint. The determination of JRC value was then investigated by many researchers (Myers 1962; Tse and Cruden 1979; Krahn and Morgenstern 1979; Feder 1988; Malinverno 1990; Lee et al. 1990; Wakabayashi and Fukushige 1992; Tatone and Grasselli 2010). Lê et al. (2018) introduced a new and simple method called profile height variation (PHV) for estimating the JRC value. The PHV method can be used to randomly generate any rock joint profile with a given JRC value. In this method, the PHV data follows the normal distribution with the zero mean and the standard deviation of the PHV. Moreover, the surface degradation and failure mechanism of a joint were well evaluated using DS tests (Usefzadeh et al. 2013; Jiang et al. 2015a; Babanouri and Karimi 2015; Pickering and Aydin 2016; Liu et al. 2017; Singh and Basu 2018; Meng et al. 2018; Le et al. 2019).

Barton (1982) found that the mobilized JRC could be predicted by linearly interpolating the peak shear displacement value using Barton's proposed table. However, the influence of normal stress and UCS on the surface roughness was not considered at the postpeak stage. Besides, the mobilized friction angle was assumed as a constant value after the peak stage, which might need to be reestimated. Asadollahi and Tonon (2010) modified the previous Barton's model based on the results of 366 DS tests. An empirical equation, which was only based on estimating the peak shear displacement, was then introduced to predict the mobilized JRC. A new table was also proposed to predict the stress–displacement curve at the prepeak stage. Amiri et al. (2014) investigated the influence of material deformability on rock joints' shear strength by performing 110 DS tests on artificial specimens. Their results indicated that the shear strength and stiffness of the stress–displacement curve were highly related to Young's modulus of joint material. Singh et al. (2017a, b) investigated the effect of irregularity depth, heterogeneity, and dynamic stress conditions on the incremental shear stress developed in irregular transversely rock media such as sandstone, granite, and marble. Furthermore, the closed-form expression of incremental shear stress was also analytically developed. The dynamic behavior of the rock medium was also evaluated and discussed through numerical computations (Singh et al. 2018; Negi et al. 2019). Liu et al. (2020) conducted 150 DS tests on artificial joint specimens to study the effect of surface degradation of such a joint during shearing. The test results implied that the mobilized JRC value strongly depended on the applied normal stress, the initial JRC value (JRC before the test), and the UCS of joint material. The mobilized friction angle was reduced at the postpeak stage, but the reason for the reduction was not explained well. Besides, their study on artificial joint specimens

[1]Postdoctoral Researcher, Dept. of Civil Engineering, National Yang Ming Chiao Tung Univ., Hsinchu City 300093, Taiwan (corresponding author). ORCID: https://orcid.org/0000-0002-9898-3337. Email: lehoangkhanhhaugiang@gmail.com

[2]Professor, Dept. of Civil Engineering, National Central Univ., Taoyuan City 320317, Taiwan. ORCID: https://orcid.org/0000-0001-9165-009X. Email: wenchaoh@g.ncu.edu.tw

[3]Professor, Dept. of Civil Engineering, National Yang Ming Chiao Tung Univ., Hsinchu City 300093, Taiwan. ORCID: https://orcid.org/0000-0002-5672-402X. Email: mcweng@nctu.edu.tw

[4]Associate Professor, Graduate Institute of Applied Geology, National Central Univ., Taoyuan City 320317, Taiwan. Email: huang22@ncu.edu.tw

Note. This manuscript was submitted on November 14, 2021; approved on February 14, 2022; published online on May 26, 2022. Discussion period open until October 26, 2022; separate discussions must be submitted for individual papers. This paper is part of the ***International Journal of Geomechanics***, © ASCE, ISSN 1532-3641.

was only based on four Barton's standard profiles, which might need to be checked and compared with more realistic profiles in the field. They also concluded that the mobilized JRC value of the specimen with large UCS decreased more significantly than that with small UCS, which might be questionable. The joint specimen's mechanical behavior with large UCS (larger than 28.62 MPa) was not investigated, which might differ from the specimens within the UCS range in their study. Most studies on estimating the postpeak shear strength of a rock joint were only based on laboratory observation. A misunderstanding of the joint's failure mechanism during shearing may lead to incorrectly predicting the mobilized JRC and friction angle. Therefore, a numerical model for simulating the mechanical behavior of the rock joint may be needed.

The behavior of rock mass containing fractures could be well simulated using the discrete element method (DEM), finite difference method (FDM), and finite element method (FEM) (Asadi et al. 2013; Liu et al. 2014; Bahaaddini et al. 2014; Jiang et al. 2015b; Guo and Qi 2015; Fan et al. 2015; Bahaaddini et al. 2016; Cheng et al. 2016; Wang et al. 2017; Lê et al. 2018; Sharma et al. 2018). Gao et al. (2019) employed the extended finite element method to simulate the behavior of fracture toughness in anisotropic material. The simulation result indicated that the development of crack paths was well predicted. Tang et al. (2019) performed the finite element meshfree modeling to explore the fracture intensity and fracture orientation of the fluid porous rock. Fei and Choo (2021) proposed the use of two phase-field models for simulating the frictional shear and cohesive tensile fractures in rocks. The proposed models showed a good estimation of fracture strength, which was independent of the phase-field length. Le et al. (2021) performed lots of lab tests and DEM simulations on artificial joint models with JRC = 19.6 using the PHV method and 3D-printing technology. Their results indicated that the DEM simulation reasonably compared well with the lab test in terms of the peak shear strength and the stress–displacement curve trend. From a microscopic viewpoint, the development of fractures, shear stress, and contact forces within the joint model was related to the applied normal stress and shear displacement. The previous discussion implies that the PHV method and DEM simulation can be used to study a rock joint's mechanical behavior under DS conditions. However, their study was only based on the soft artificial rock joint with very low strength (UCS = 4.42 MPa). The influence of the JRC and UCS on the peak and residual shear strength of a rock joint was also not investigated.

Therefore, this study investigated JRC and UCS's effect on the peak and residual shear strength of rock joints through a series of physical and numerical models. Artificial joint specimens with different JRC values (20, 19.6, and 10) were replicated using the PHV method (Lê et al. 2018, 2021) and 3D-printing technology. The UCS of artificial material (a mixture of cement, sand, and water) was 37.1 MPa (rock mass with medium strength in ISRM classification). The joint surfaces of all specimens before and after the tests were scanned using blue LED projection technology to determine the actual JRC value. Afterward, a 2D particle flow code software (PFC2D version 5.0 by Itasca 2017) was used to simulate rock joints' mechanical behavior under DS conditions. The joint surface in 2D DEM was modeled based on the actual scanned profile obtained from the laboratory. DS tests on artificial joint models were performed under different normal stresses (0.4, 1, and 2 MPa). The lab test results were then used to validate the 2D DEM model in terms of the peak shear strength and the stress–displacement curve. The failure mechanism and shear strength of the joint was then discussed based on the observation of lab tests and 2D DEM simulations. The characteristics of mobilized JRC and mobilized friction angle at the residual stage were also evaluated and explained from the microscopic viewpoint. Finally, a new equation for predicting the residual shear strength of a rock joint was proposed.

## Methodology

### Preparation of Artificial Joint Specimens with Different Joint Profiles

This study extends the study of Le et al. (2021), the influence of surface roughness on the peak and residual shear strength of a rock joint was investigated using three previous randomly generated profiles. The 2D joint profiles with JRC = 20 [Fig. 1(a)] and JRC = 10 present the high and moderate JRC values. The dimension of the 3D profile with JRC = 20 was illustrated in Fig. 1(b), which was formed based on the 2D profile. The 3D model block with a given joint surface could be printed using the above 3D profile and 3D-printing technology [Fig. 1(c)]. The 3D block was then positioned inside the acrylic box for casting purposes [Fig. 1(d)]. An artificial joint specimen with a particular JRC value could be cast by slowly pouring cement material into the box. The cement material was a mixture of cement, sand, and water with the specified mixing ratio by weight (1:1:0.6). The UCS of the cement specimen, which presented cement material strength, was determined based on the UCS test. The average UCS of cement mixture was determined as 37.1 MPa, which was classified as moderate rock strength (ISRM classification). Besides, the artificial joint cement specimen with JRC = 19.6 was also cast to compare the mechanical behavior with the gypsum material from the previous study (Le et al. 2021) under the same JRC value. Artificial cement specimens after casting were shown in Figs. 2(a–c). A joint specimen before and after the test was scanned to calculate the actual JRC value (Fig. 3). For each specimen, the surfaces of the lower and upper parts were both scanned. However, in this study, the scanning result from the lower part was mainly estimated. A total of nine profiles with an equal space (1.2 cm) were chosen from the joint surface, as illustrated in Fig. 2(d). The scan result of all artificial cement specimens before the test is shown in Table 1. The JRC values of the joint profiles with JRC = 19.6, JRC = 20, and JRC = 10 (initial values) were reevaluated as 11, 10, and 2.4, respectively. The JRC reduction of cement specimens is larger than that of gypsum specimens (Le et al. 2021). The reason may be due to the shrinkage process of the cement mixture during and after replicating. Barton's equation could later reexamine the peak shear strength of a rock joint obtained from the lab test based on the actual JRC value.

### Formation of a 2D-DEM Joint Model with Scanned JRC

To simulate cement material in 2D DEM, the UCS of the numerical model should be similar to that of actual cement specimens. The numerical model of the UCS test was first performed to validate with the laboratory tests. The UCS model size was 50 mm in width and 125 mm in height, which was simulated using 112,132 particles with a uniform radius of 0.125 mm (Fig. 4). In the laboratory, the UCS test was conducted using stress-controlled equipment with the measurement of peak strength only (a limitation of our current apparatus). Therefore, the calibration of the UCS simulation was only performed on the peak strength. The simulated UCS model was compressed at a constant strain rate of 0.021 mm/s until the peak strength was reached. The particle assembly was connected using the parallel bond model. Some micro parameters such as the effective Young's modulus, bond stiffness, tensile strength, cohesion, and friction coefficient in the parallel bond model highly control the UCS of a rock sample in 2D-DEM simulation. The linear

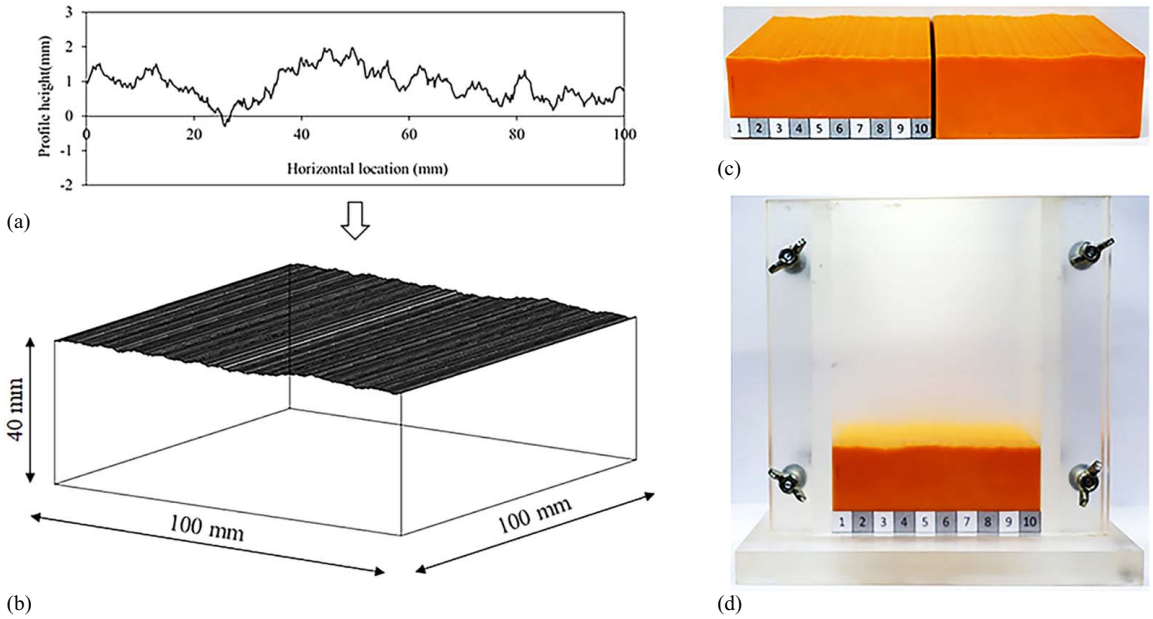


**Fig. 1.** Preparation of 3D model block using 3D-printing technology: (a) 2D joint profile with JRC = 20; (b) 3D joint profile with JRC = 20; (c) 3D printed model block; and (d) acrylic box.

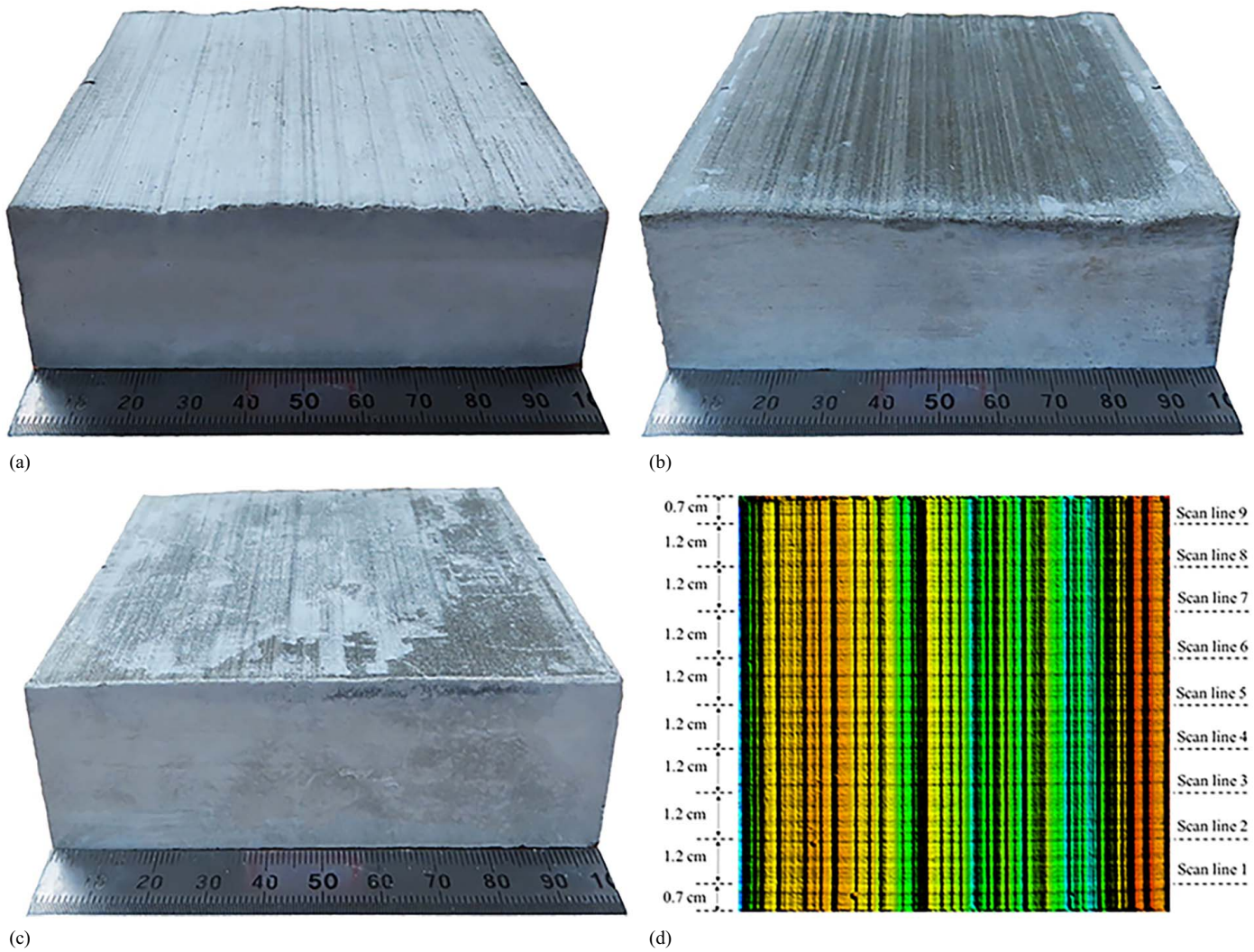


**Fig. 2.** Artificially cast cement specimens with given JRCs: (a) JRC = 20; (b) JRC = 19.6; (c) JRC = 10; and (d) location of scan lines.

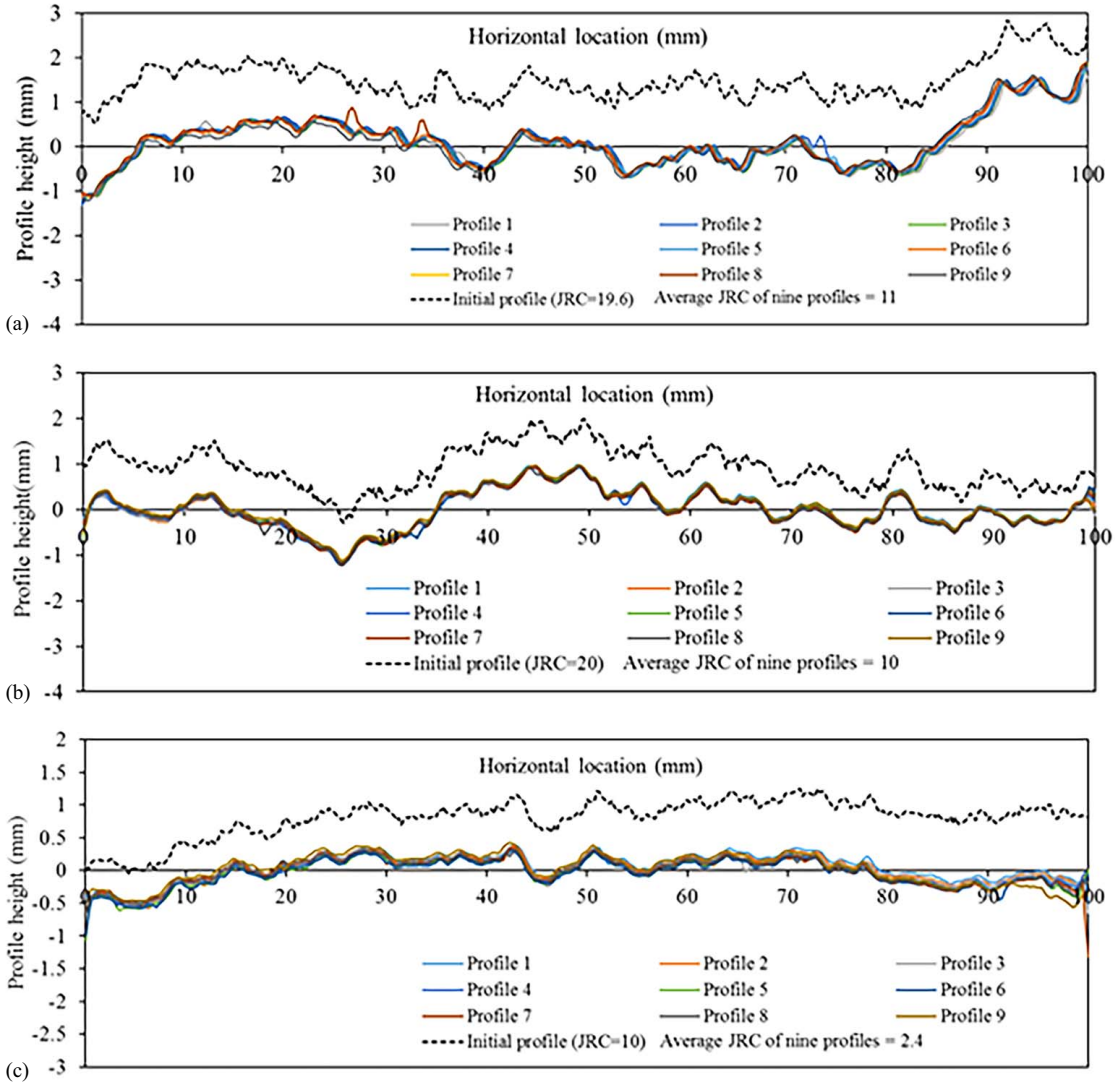


**Fig. 3.** Scanned profile of the cement specimens before the test and the comparison with initial profiles: (a) given JRC = 19.6, actual JRC = 11; (b) given JRC = 20, actual JRC = 10; and (c) given JRC = 10, actual JRC = 2.4.

**Table 1.** Actual JRC value of artificial joint specimens after replicating

| Reduction of JRC after replicating | | |
|---|---|---|
| Material used | Given JRC | Scanned JRC |
| Gypsum (Le et al. 2021) | 19.6 | 16.8 |
| Cement (this study) | 20 | 10 |
| | 19.6 | 11 |
| | 10 | 2.4 |

contact model was also used to simulate the force-displacement interaction between particle and wall or amongst particles when the parallel bond contact was broken. The above parameters were evaluated and chosen based on trials and errors in comparing the strength and failure mode between lab tests and simulations. Table 2 shows the calibrated parameters used in this study.

A rock joint's mechanical behavior could be investigated based on nine DS tests in 2D DEM simulation. Each 2D DEM model with 100 × 70 mm in dimensions contained 32,352 particles with a radius of 0.125 mm and 24,032 particles with a radius of 0.25 mm.

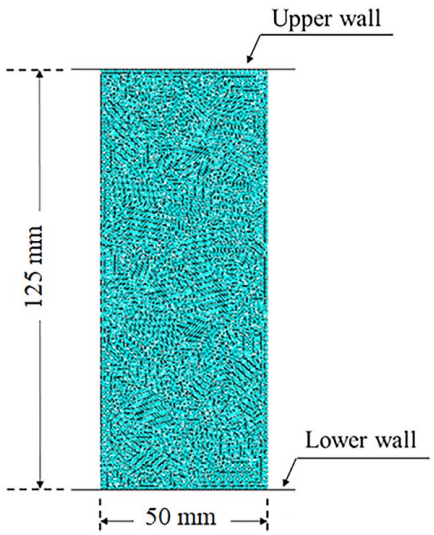


**Fig. 4.** Dimensions of UCS model in 2D-DEM.

The use of different particle sizes in the DS simulation was well discussed by Lê et al. (2018, 2021). Afterward, the joint profile with actual JRC values (10, 11, and 2.4) obtained from the artificial specimens' scanning result was generated in the middle of the 2D DEM model. In each joint model, 399 small fractures with given coordinates were generated using the smooth joint model to form the joint surface. The fracture in the 2D DEM model is represented by three components including the fracture center, length of fracture, and dip direction [Fig. 5(a)]. Therefore, the change of the three components of fractures will accordingly change the roughness of the joint surface (the JRC value). The complete 2D-DEM models with given JRC values (10, 11, and 2.4) are illustrated in Figs. 5(b–d). The polylines in the middle of the models present the joint surface. The smooth joint model's properties, including the joint stiffness and friction coefficient, strongly influence the joint surface's shear behavior. The joint models were sheared at a constant velocity of 0.0083 mm/s under different normal stresses (0.4, 1, and 2 MPa) in laboratory tests and numerical simulations. A DS test could be terminated when the shear displacement reached 10 mm. In this study, hundreds of UCS and DS simulations were performed to adjust the 2D DEM model parameters. The final set of parameters (Table 2) was selected when consistent results regarding the strength, failure type, and stress–displacement trend between lab tests and simulations were obtained. The number of broken bonds was evaluated during shearing to explore the rock joint's failure mechanism under DS conditions. After shearing, the upper part of the DS model was detached from the lower part. The actual JRC value of the 2D DEM models was then determined for further comparison with lab tests.

**Table 2.** Parameters in the 2D-DEM model with UCS = 36.9 MPa

| Model | Particle property | Values |
|---|---|---|
| Linear contact | Effective modulus ($N/m^2$) | $3.6 \times 10^8$ |
| | Normal to shear stiffness ratio (–) | 2.5 |
| | Friction coefficient | 0.5 |
| Linear parallel bond | Bond effective modulus ($N/m^2$) | $9 \times 10^7$ |
| | Normal to shear stiffness ratio (–) | 2.5 |
| | Critical damping ratio (–) | 0.05 |
| | Tensile strength (Pa) | $3.2 \times 10^7$ |
| | Cohesion (Pa) | $3.2 \times 10^7$ |
| | Friction angle (degrees) | 0 |
| Smooth joint | Normal stiffness per unit area ($N/m^3$) | $1 \times 10^6$ |
| | Shear stiffness per unit area ($N/m^3$) | $1 \times 10^6$ |
| | Friction coefficient (–) | 0.7 |

## DS Results and Verification of 2D DEM Models

In the laboratory, the average UCS of the cement specimens was approximately 37.1 MPa. The UCS of the 2D DEM model with the parameters in Table 2 was 36.9 MPa, consistent with the laboratory results. Figs. 6(a and b) compares the UCS specimen's failure

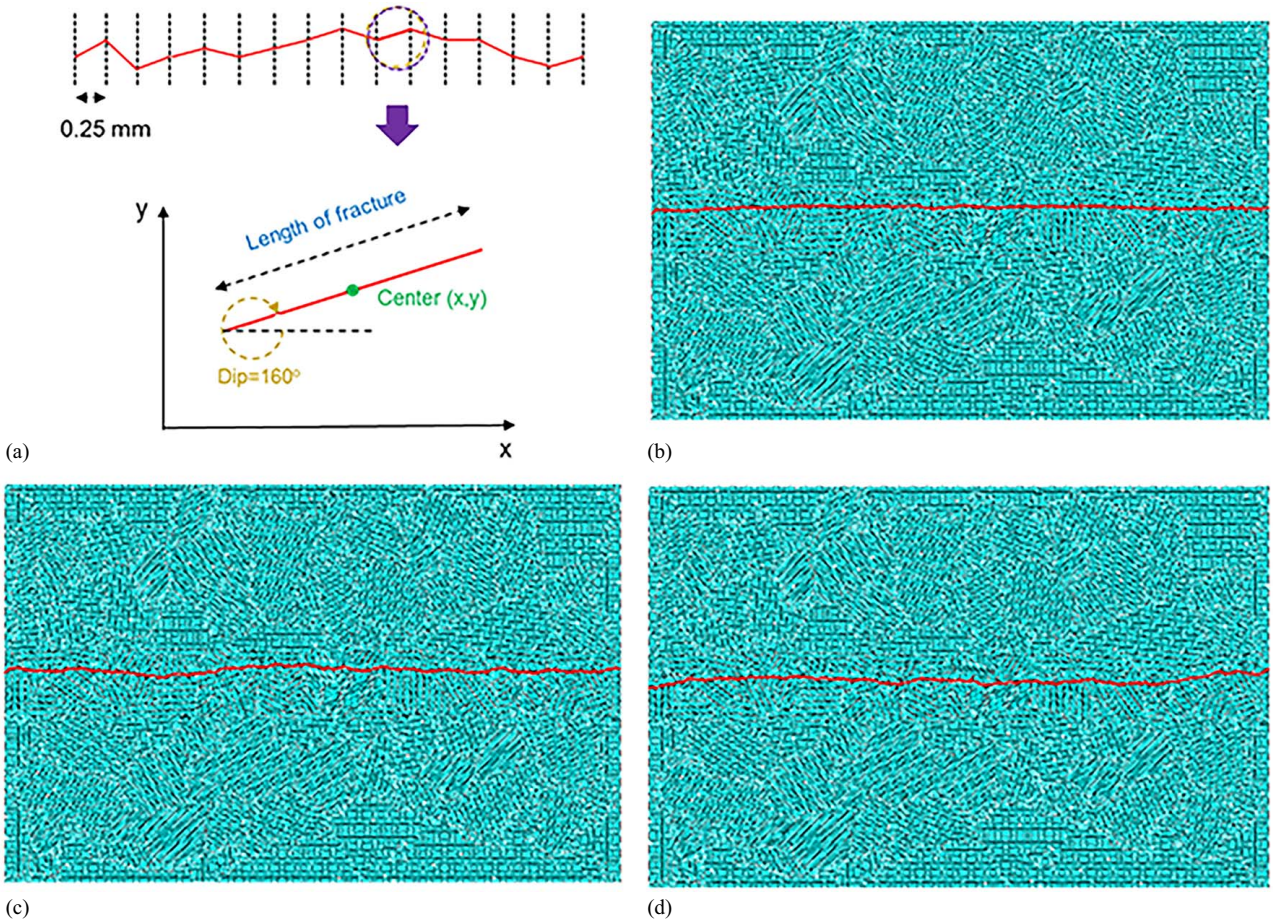


**Fig. 5.** Simulation of the joint with actual JRC in 2D-DEM: (a) details of fracture formation; (b) joint profile with JRC = 2.4 (No. of parallel bonded contact = 112,742; No. of smooth joint contact = 17,056); (c) joint profile with JRC = 10 (No. of parallel bonded contact = 109,766 and No. of smooth joint contact = 19,098); and (d) joint profile with JRC = 11 (No. of parallel bonded contact = 110,774 and No. of smooth joint contact = 14,387).

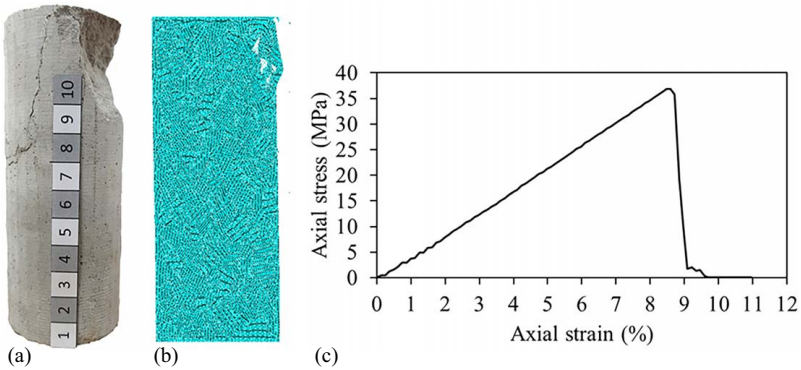


**Fig. 6.** Results of UCS test: (a) cement plaster specimen at failure; (b) simulated specimen at failure; and (c) the stress–strain curve of UCS simulation.

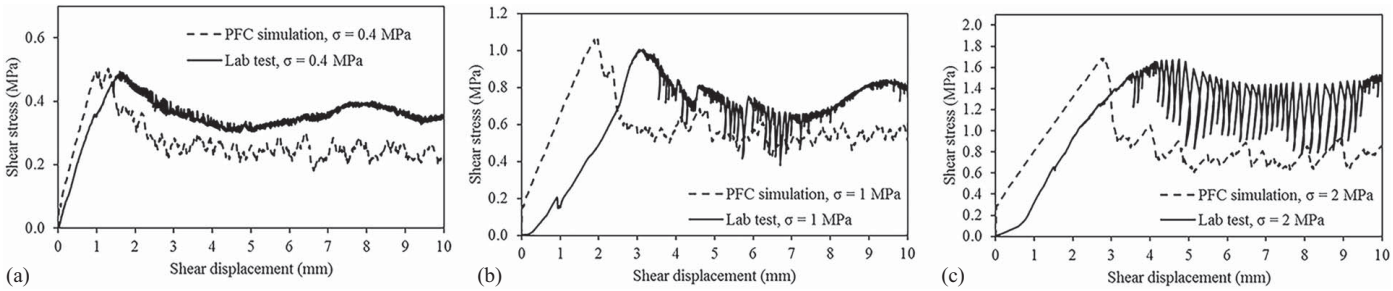


**Fig. 7.** Comparison of DS test results for the cement and 2D-DEM models with JRC = 2.4 under different normal stresses: (a) 0.4 MPa; (b) 1 MPa; and (c) 2 MPa.

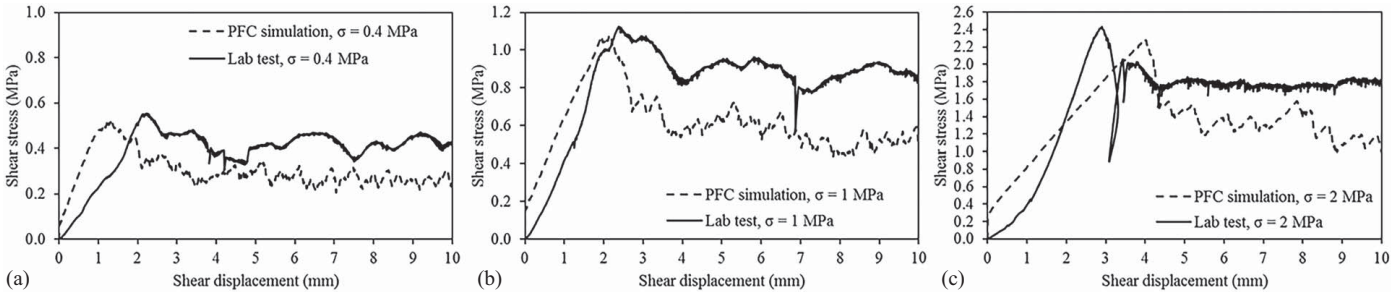


**Fig. 8.** Comparison of DS test results for the cement and 2D-DEM models with JRC = 10 under different normal stresses: (a) 0.4 MPa; (b) 1 MPa; and (c) 2 MPa.

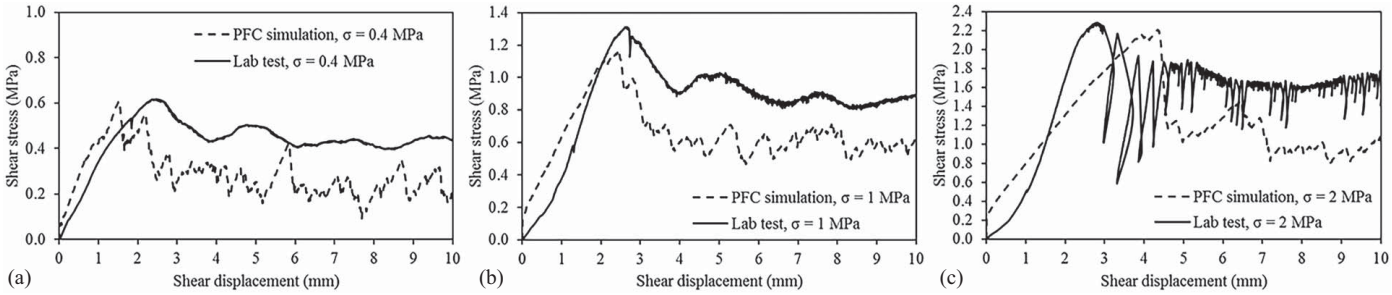


**Fig. 9.** Comparison of DS test results for the cement and 2D-DEM models with JRC = 11 under different normal stresses: (a) 0.4 MPa; (b) 1 MPa; and (c) 2 MPa.

conditions between lab tests and numerical simulation. A similar crack at the top-right side of the two models was observed. The typical stress–strain curve of the UCS model in 2D DEM was also depicted in Fig. 6(c). The peak strength was reached at the axial strain of 8.5%. Therefore, the simulated model could be classified as the medium-strength rock with highly yielding based on Deere and Miller (1996) classification. The results indicated that the 2D DEM could well simulate a rock mass's mechanical behaviors.

**Table 3.** Comparisons on the peak shear strength of cement specimens amongst lab tests, Barton's formula, and 2D-DEM simulation

| UCS (MPa) | Basic friction angle (degree) | Given JRC | Actual JRC before test | Normal stress (MPa) | Peak shear strength of joint model (MPa) | | |
|---|---|---|---|---|---|---|---|
| | | | | | Lab test | Barton's formula and percentage difference (%) | 2D-DEM simulation percentage difference (%) |
| 37 | 37 | 20.00 | 10.00 | 0.40 | 0.55 | 0.61 (−9.55%) | 0.52 (5.77%) |
| | | | 10.00 | 1.00 | 1.12 | 1.31 (−14.62%) | 1.07 (4.67%) |
| | | | 10.00 | 2.00 | 2.43 | 2.36 (3.14%) | 2.29 (6.11%) |
| | | 19.60 | 11.00 | 0.40 | 0.62 | 0.66 (−5.49) | 0.61 (1.64%) |
| | | | 11.00 | 1.00 | 1.31 | 1.39 (−5.69%) | 1.17 (11.97%) |
| | | | 11.00 | 2.00 | 2.29 | 2.46 (−7.08%) | 2.21 (3.62%) |
| | | 10.00 | 2.4 | 0.40 | 0.49 | 0.44 (11.04%) | 0.5 (−2.00%) |
| | | | 2.4 | 1.00 | 1.00 | 0.86 (16.19%) | 1.06 (−5.66%) |
| | | | 2.4 | 2.00 | 1.67 | 1.68 (−0.50%) | 1.69 (−1.18%) |

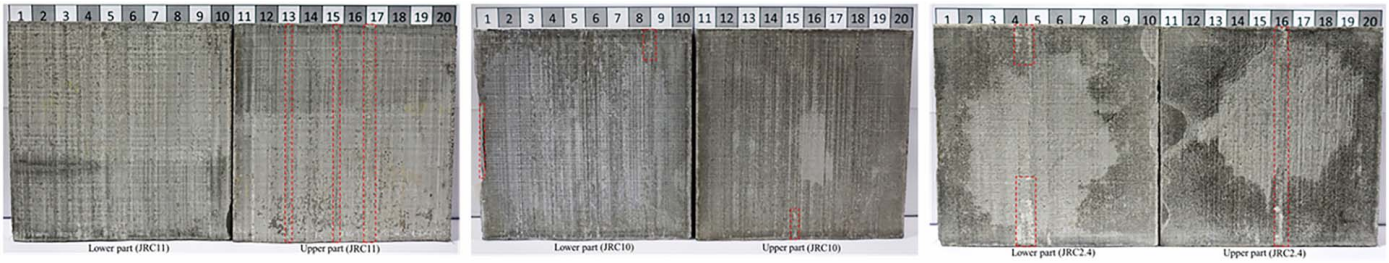


(a) (b) (c)

**Fig. 10.** Top views of postshearing profile with different JRCs under normal stress of 0.4 MPa: (a) JRC = 11; (b) JRC = 10; and (c) JRC = 2.4.

Figs. 7–9 compare the DS results between lab tests and numerical simulation. The difference in the peak shear strength amongst lab tests, Barton's prediction, and numerical simulation was presented in Table 3. With the given JRC values and basic friction angle, the peak shear strength of a rock joint could be calculated using Barton's formula. The basic friction angle, which was determined based on the DS test of a flat joint surface model, was 37°. Table 3 implied that most lab tests showed a good comparison of the peak shear strength with Barton's estimation (less than 10% difference). The maximum differences are 14.62% and 16.19% for the lab tests with JRC = 10 and 2.4 under 1 MPa normal stress, which can be acceptable. The peak shear strength of 2D-DEM models with JRC = 2.4 (Fig. 7) under different normal stresses (0.4, 1, and 2 MPa) was 0.5, 1.06, and 1.69 MPa, respectively. The result indicates that the peak shear strength of 2D-DEM models with JRC = 2.4 is similar to that in the laboratory, especially under 2 MPa normal stress. The maximum difference between the lab test and 2D-DEM simulation is only 5.7% under the normal stress of 1 MPa. Under 1 and 2 MPa normal stress, although the lab test's peak shear strength is reached at a higher shear displacement than that of the 2D-DEM simulation, the slope of the prepeak stress–displacement curve is almost the same. The difference in the peak shear displacements (shear displacement value at the peak shear strength) between the lab test and simulation may be attributed to the imperfect contact of the lower and upper parts of the laboratory's joint specimens. Therefore, when the joint specimen is sheared, additional shear displacement is required to make the joint in perfect contact and to reach the peak shear strength. The lab test and 2D-DEM models with JRC = 10 are shown in Fig. 8. Under 0.4, 1, and 2 MPa normal stress, the differences in the peak shear strength between the lab test and simulation are 5.8%, 4.7%, and 6.1%, which implies a good comparison. Although the trend of stress–displacement curves in the 2D-DEM model under 2 MPa show a slight difference with the lab test, most of the tests indicate a reasonable comparison. Fig. 9 shows the stress–displacement curves of the joint model with JRC = 11. Under 0.4 and 2 MPa normal stress, there is almost no difference in the peak shear strength between the lab test and the simulation. Under 1 MPa normal stress, the difference in the peak shear strength is about 12%, which is still within the acceptable value range. The previous discussion indicates that the 2D-DEM model with a randomly generated profile can be used to explore the rock joint's micromechanical behaviors during and after shearing, especially for two distinct materials. The lab test result was then used for further analysis, such as estimation of residual shear strength.

## Mechanical Behavior of the Artificially Jointed Cement Models

### *Lab Test Results*

To better evaluate the UCS, JRC, and normal stress on the shear strength of the joint, top-view photographs of the sheared profiles of cement specimens with different JRC values (11, 10, and 2.4) after the test are illustrated in Figs. (10)–(12). In each photo [Fig. 10(a)], the lower part of the cement specimen is depicted on the left-hand side, and the upper part is depicted on the right-hand side. The joint surface's damaged area is marked with the dashed rectangles to easily investigate the detailed variations of the joint profile after shearing. The damage ratio of the joint surface of cement specimens, which equals the damaged area divided by the total area, is also calculated and compared in Table 4. Overall, under the same normal stress, the joint surfaces' damage ratio decreases with the decrease of the JRC values. With the increase of normal stress, a higher damage ratio or more damage can be observed. Under the normal stress of 0.4 MPa, the cement sample reveals slight damage at a few local parts of the specimen. In contrast,

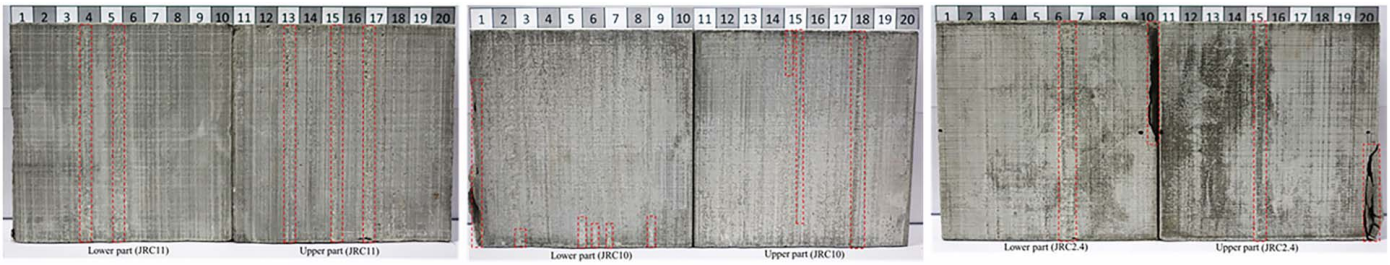


(a) (b) (c)

**Fig. 11.** Top views of postshearing profile with different JRCs under normal stress of 1 MPa: (a) JRC = 11; (b) JRC = 10; and (c) JRC = 2.4.

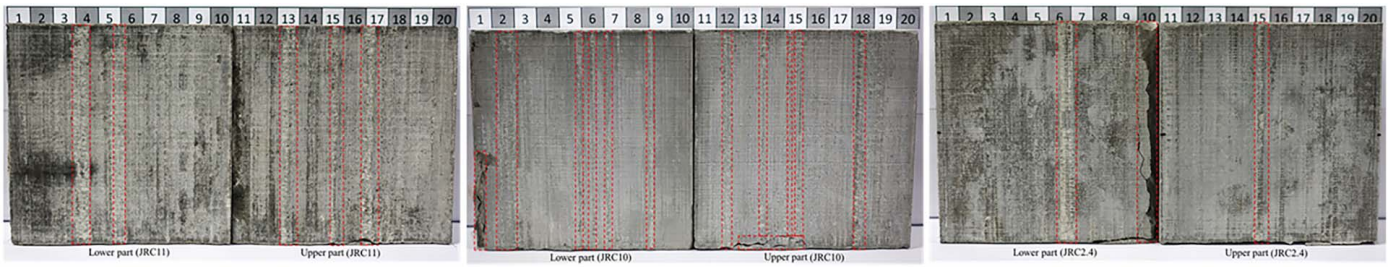


(a) (b) (c)

**Fig. 12.** Top views of postshearing profile with different JRCs under normal stress of 1 MPa: (a) JRC = 11; (b) JRC = 10; and (c) JRC = 2.4.

**Table 4.** Damage ratio of cement specimens and comparison with gypsum specimen (Le et al. 2021)

| Normal stress (MPa) | Cement specimen (%) (this study) | | | Gypsum specimen (%) (Le et al. 2021) |
|---|---|---|---|---|
| | JRC = 11 | JRC = 10 | JRC = 2.4 | JRC = 16.8 |
| 0.40 | 8.60 | 1.80 | 6.40 | 15.85 |
| 1.00 | 15.90 | 10.15 | 8.03 | 53.80 |
| 2.00 | 22.12 | 20.92 | 17.66 | 69.40 |

the remaining parts clearly retain the joint surface's shape, indicating that the shearing resistance may come from the relative sliding between the specimen's lower and upper parts. Under low normal stress, the shear strength of the artificial cement specimen may be only mobilized from the frictional property of such a joint. The joint cement specimens' mechanical behavior is similar to what is observed for the gypsum specimen under low normal stress. However, under high normal stress, mechanical behavior may be a slight difference. Under 1 MPa normal stress, the damage ratio of cement specimens with different JRC varies from 8% to 16%, which indicates that more damages are observed. In this case, the frictional characteristic and the joint profile's cohesion may both contribute to the shear strength of artificial cement specimens. Under the normal stress of 2 MPa, the average damage ratio of all cement specimens is about 20%, which implies that the contribution of cohesion to the shear strength of cement specimens increases. Under high normal stress, the gypsum specimen's joint profile is almost sheared (damage ratio = 69.4%), while that of the cement specimen is slightly sheared. The difference in failure behaviors of gypsum and cement specimens during shearing may be due to the difference in the UCS of the two materials. Under low UCS (4.42 MPa), the joint gypsum specimens' shear strength is mostly mobilized from the gypsum material's cohesion under high normal stress (2 MPa). However, for the cement specimens under the same stress condition, most of the shear strength comes from the joint profile's frictional properties.

### *DEM Simulation*

The rock joint's failure mechanism is further investigated from the microscopic viewpoint in the 2D DEM simulation. Fig. 13 shows the accumulation of fractures of the joint profile in different models under 1 MPa normal stress. The result indicates that the number of fractures in cement models is much smaller than that in gypsum models (Le et al. 2021). This difference may be attributed to the low ratio, 0.027, of normal stress to UCS of simulated cement material. Under different normal stresses, there are almost no fractures formed at the peak shear strength stage. The previous observation implies that cement models' peak shear strength mainly comes from the friction along with the joint profile, which is similar to gypsum models' behavior. Afterward, fractures begin to develop at the residual stage (5 and 10 mm shear displacements), but the number of fractures is very small. The result proves that the residual shear strength mostly arises from the friction while the contribution of cohesion is insignificant, which is different from gypsum models. A similar fracture development trend was also observed for cement models under 0.4 and 2 MPa normal stresses. The above discussions indicate that the UCS of the simulated model is related to the failure mechanism and the shear strength development of the joint model under DS condition. The development of fractures was also estimated by recording the number of broken bonds of the connected particles during shearing (Fig. 14). For cement models, the number of broken bonds is much smaller than that of the gypsum model, which may be due to the high UCS of simulating material. Under the same UCS (36.9 MPa), the model with a large JRC value shows more broken bonds (or fractures) than the model with a small JRC value. For example, under 2 MPa normal stress, the percentages of broken bonds of the 2D-DEM models with JRC = 2.4, JRC = 10, and JRC = 11 are 0.2%, 0.28%, and 0.36%, respectively. The above discussion indicates that the rock joint's failure mechanism during shearing is associated with the joint profile's roughness and normal stress applied to the model.

Fig. 15 shows the observation of joint surfaces at different stages of shearing in the 2D DEM models. All models show that

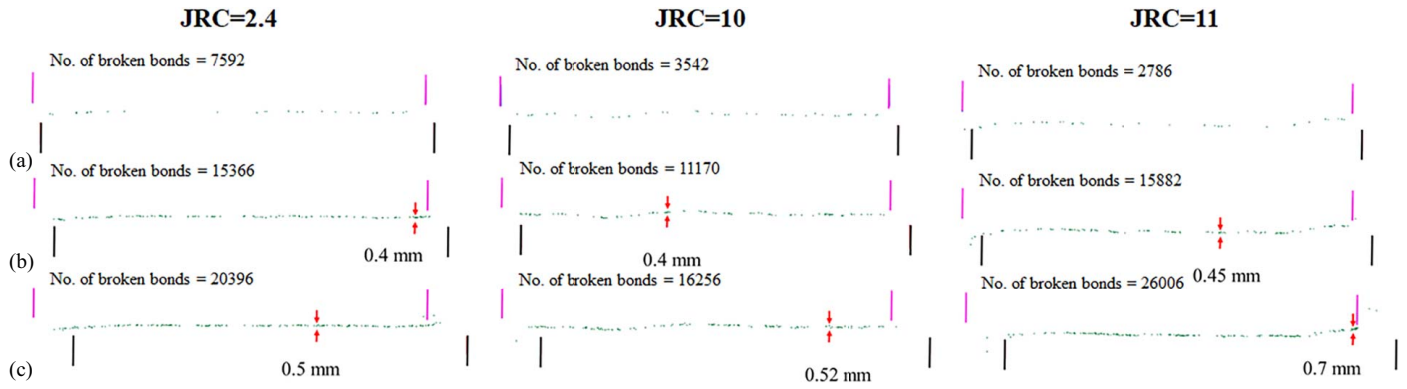


**Fig. 13.** Accumulation of broken bonds along with the joint profile of different 2D-DEM models under the normal stress of 1 MPa at various shear displacements: (a) displacement at peak shear stress; (b) 5 mm; and (c) 10 mm.

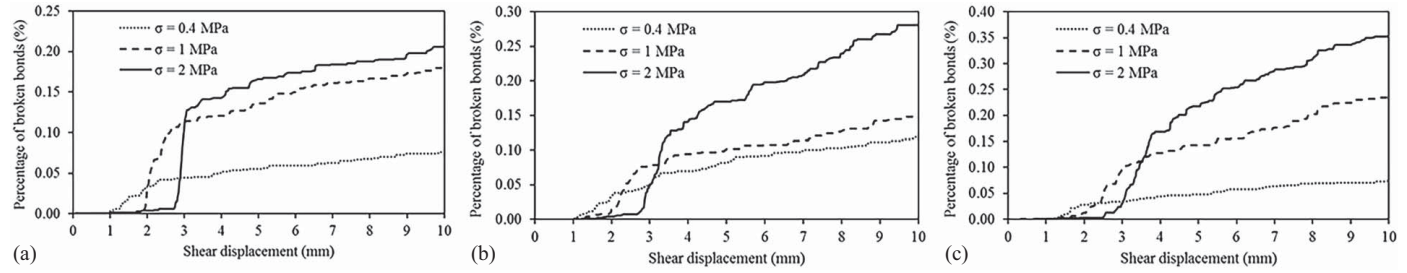


**Fig. 14.** Percentage of broken bonds of different 2D-DEM models under various normal stresses during shearing: (a) models with JRC = 2.4; (b) models with JRC = 10; and (c) models with JRC = 11.

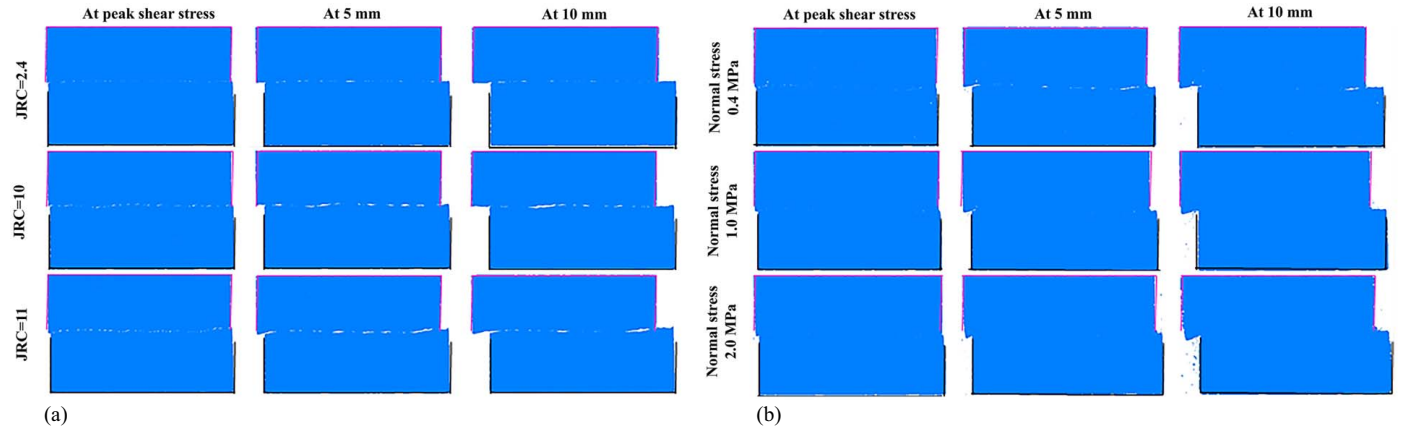


**Fig. 15.** Shearing process of 2D DEM models: (a) cement models; and (b) gypsum models (data from Le et al. 2021).

the lower and upper surfaces are well contacted at the peak stage without any gaps. The result proves that the basic friction angle is fully mobilized at the peak stage, which agrees well with the lab observation from previous studies (Barton 1982; Asadollahi and Tonon 2010; Liu et al. 2020). For cement models [Fig. 15(a)], many gaps along with joint surfaces are obvious due to dilation (5 and 10 mm shear displacement), which may cause the shear strength reduction at the residual stage. The degree of dilation highly depends on the joint roughness. In this case, the basic friction angle may not be fully mobilized because the contact area is partially decreased. For gypsum models at the residual stage [Fig. 15(b)], dilation behavior is also observed under 0.4 MPa normal stress, similar to cement models. However, under 1 and 2 MPa normal stress, gypsum models' basic friction angle may be fully mobilized. The above discussion indicates that the investigation of mobilized JRC and mobilized friction angle plays a vital role in estimating a rock joint's residual shear strength.

## Estimation of Residual Shear Strength

### *Mobilized JRC*

All artificial joint specimens after the shear test were scanned to evaluate the joint surface degradation. The scanned results indicated that the mobilized JRC was related to the normal stress and the UCS of cement specimens (Table 5). Under large normal stress, the reduction rate of the JRC is higher than that under small normal

**Table 5.** Actual JRC of cement models after the test

| UCS (MPa) | Given JRC | Normal stress (MPa) | Actual JRC before test | Actual JRC after test | Reduction rate (%) |
|---|---|---|---|---|---|
| 37 | 20.00 | 0.40 | 10.00 | 8.40 | 16.00 |
| | | 1.00 | 10.00 | 8.36 | 16.40 |
| | | 2.00 | 10.00 | 8.25 | 17.50 |
| | 19.60 | 0.40 | 11.00 | 9.96 | 9.45 |
| | | 1.00 | 11.00 | 9.77 | 11.18 |
| | | 2.00 | 11.00 | 9.01 | 18.09 |
| | 10.00 | 0.40 | 2.40 | 1.77 | 26.25 |
| | | 1.00 | 2.40 | 1.59 | 33.75 |
| | | 2.00 | 2.40 | 1.52 | 36.67 |

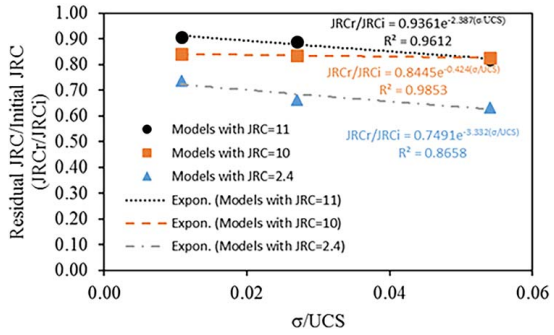


**Fig. 16.** Relationship between residual JRC and initial JRC with respect to the normal stress and UCS ratio of artificial cement specimens.

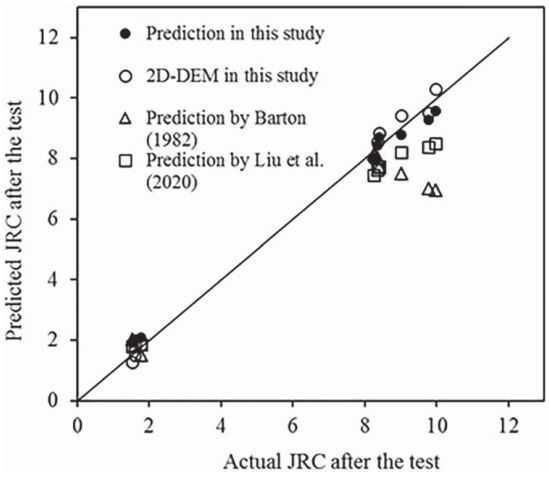


**Fig. 17.** Estimation of the JRC after the test.

stress. The relationship between the actual JRC and the $\sigma$/UCS ratio is shown in Fig. 16. For each group of the initial JRC, the above relationship is represented by an exponential equation. The prediction of mobilized JRC can be constructed by taking the average value of constant parameters of three exponential equations in Fig. 16. Some minor adjustments of constant parameters are then performed based on lab test results to obtain Eq. (1). The predicted JRC from Eq. (1) was then compared with the results using Liu et al.'s model (2020), and Barton's model (1982) (Fig. 17). The analyzed results imply that all models may predict well the mobilized JRC under a small initial JRC value. However, for high initial JRC values, the result obtained from this study shows an improved prediction in comparison to that using Liu et al.'s model. The reason may be due to the high UCS (37.1 MPa) of cement specimens in this study. Besides, the mobilized JRC predicted by Eq. (1) also shows a good agreement with that obtained from the 2D DEM models after shearing. A significant discrepancy in the prediction of Barton's model exists under high initial JRC values.

$$\mathrm{JRC}_{\mathrm{predicted}} = \mathrm{JRC}_{\mathrm{initial}} \times 0.895 e^{-2.048\frac{\sigma}{\mathrm{UCS}}} \quad (1)$$

### Mobilized Friction Angle

Many previous studies showed that the basic friction angle remained a constant value during shearing until the end of the test (Barton 1982). However, Liu et al. (2020) indicated that the joint's friction angle was decreased based on their lab test results. In this study, the friction angle's influence was investigated using Eq. (2), which was based on the transformation of Barton's model. In the equation, the residual shear strength $\tau_{\mathrm{residual}}$ was obtained based on the stress–strain curve of cement specimens at the postpeak strength stage. Besides, the actual JRC value of joint surfaces after the test was also taken into account. The calculation results are illustrated in Table 6. A new term called deduction factor D, which was defined as the ratio of the mobilized friction angle to the initial basic friction angle, was also calculated. The analyzed result implies that the friction angle is reduced from the initial basic friction value to a certain value, which is independent of the normal stresses applied to the specimens. The reason for the reduction of friction angle may be due to the following reasons. The basic friction angle was obtained based on the direct shear test of the flat joint model. During shearing, the artificial specimen's lower and upper parts were perfectly connected until the test is terminated. However, the above perfect connection was only observed at the shearing process's prepeak stage for the specimens with given JRC values (11, 10, and 2.4). After the peak shear strength was obtained, the joint surface began to be sheared, which also depended on the initial JRC value and the UCS of the material. Therefore, the connection between the lower and upper parts of the specimen

**Table 6.** Estimation of the mobilized friction angle

| Basic friction angle $\phi_0$ (degree) | UCS (MPa) | Given JRC | Actual JRC before the test | Normal stress (MPa) | Actual JRC after the test | Residual shear strength from Lab test (MPa) | Estimation of mobilized friction angle $\phi_1$ (degree) | Deduction factor $D = \phi_1/\phi_0$ | Average value of $D$ | Standard deviation of $D$ |
|---|---|---|---|---|---|---|---|---|---|---|
| 37 | 37 | 20 | 10 | 0.4 | 8.4 | 0.43 | 31.85 | 0.83 | 0.82 | 0.012 |
| | | | | 1 | 8.36 | 0.93 | 29.81 | 0.81 | | |
| | | | | 2 | 8.25 | 1.75 | 31.21 | 0.83 | | |
| | | 19.6 | 11 | 0.4 | 9.96 | 0.44 | 28.14 | 0.76 | 0.77 | 0.011 |
| | | | | 1 | 9.77 | 0.96 | 28.51 | 0.77 | | |
| | | | | 2 | 9.01 | 1.70 | 28.95 | 0.78 | | |
| | | 10 | 2.4 | 0.4 | 1.77 | 0.31 | 34.30 | 0.93 | 0.92 | 0.006 |
| | | | | 1 | 1.59 | 0.74 | 34.01 | 0.92 | | |
| | | | | 2 | 1.52 | 1.44 | 33.83 | 0.91 | | |

might not be good because of the surface damage and the dilation behavior. The effect of initial JRC on the deduction factor $D$ was also evaluated in Fig. 18. The joint profile with a large initial JRC value showed a higher reduction than that with a small initial JRC value. The mobilized friction angle at the residual stage was found to be associated with the initial JRC value [Eq. (3)]. The back-calculation of mobilized friction angle using different models is shown in Table 7. Barton (1982) assumed that at the residual stage, the mobilized friction angle was equal to the basic friction angle. The results indicate that Barton's prediction shows a large difference in the mobilized friction angle compared to the lab test calculation. The prediction using Eq. (3) shows the best result. Finally, Eq. (4) was introduced to predict the joint's residual shear strength.

$$\phi_1 = \tan^{-1}\left(\frac{\tau}{\sigma_n}\right) - \mathrm{JRC}\log_{10}\left(\frac{\mathrm{UCS}}{\sigma_n}\right) \tag{2}$$

$$\phi_{\mathrm{mobilized}} = \varnothing_{\mathrm{initial}} \times D = \varnothing_{\mathrm{initial}} \times 0.9646e^{-0.019\mathrm{JRC}_{\mathrm{initial}}} \tag{3}$$

$$\tau_{\mathrm{residual}} = \sigma_n \tan\left[\left(\mathrm{JRC}_{\mathrm{initial}} \times 0.895e^{-2.048\frac{\sigma_n}{\mathrm{UCS}}}\right)\log_{10}\left(\frac{\mathrm{UCS}}{\sigma_n}\right) + \varnothing_{\mathrm{initial}} \times 0.9646e^{-0.019\mathrm{JRC}_{\mathrm{initial}}}\right] \tag{4}$$

## Verification of the Proposed Model

### Lab Test Results in This Study

The residual shear strength of lab tests was used to verify the proposed model [Eq. (4)] in this study. The prediction of shear strength from Eq. (4) was compared with that from Liu et al. (2020) and Barton (1982) in Fig. 19. The results from Eq. (4) show a more accurate prediction than other models. Barton's model overestimates the residual shear strength, while the Liu et al. (2020) model shows an underestimation. Therefore, the proposed model of residual shear strength can be applied within the UCS ranged 0–37.1 MPa, even higher.

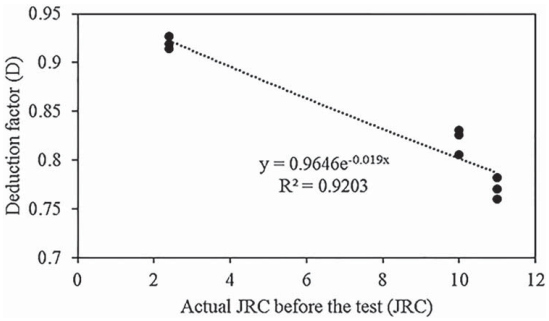


**Fig. 18.** Reduction of basic friction angle in the residual stage.

### Lab Test Results by Liu et al. (2020)

Liu et al. (2020) proposed a new model for estimating the postpeak shear strength of artificial joint specimens (eight test groups). The lab results were then compared with their proposed model, Barton's model (1982), and Asadollahi and Tonon's model (2010). Their comparisons indicated that different models showed different fluctuations in both the peak and residual shear strength to the lab test results. In this study, the lab tests' residual shear strength at the shear displacement of 9.6 mm was collected from Liu et al.'s study to compare with the prediction result using Eq. (4) (Table 8). The initial JRC value for each test was collected from their test data, and the basic friction angle was also calculated. With known initial JRC value and basic friction angle, the residual shear strength at 9.6 shear displacement could be predicted using Eq. (4), as shown in Table 8. The estimated residual shear strength in this study compared well with that of the lab test results by Liu et al. (2020). The difference between the lab test and the prediction is less than 6% for different test groups (A2, A3, A4, B2, B3, and B4), while the maximum difference of Liu's model, Barton's model, and Asadollahi's model are 13.5%, 17.07%, and 18.32%, respectively. For other test groups (C3, C4), Barton's model and Asadollahi's model highly overestimated the joint's residual shear strength; the maximum differences are 68.23%, 59.11%, respectively. However, this study and Liu's model show a better prediction, although the maximum differences are still large for test group C4 (38.63% and 36.11%). The reason may be due to the high normal stress, which is applied to the specimens. The $\sigma_n$/UCS ratio should be ranged between 0.001 and 0.1 (Asadollahi and

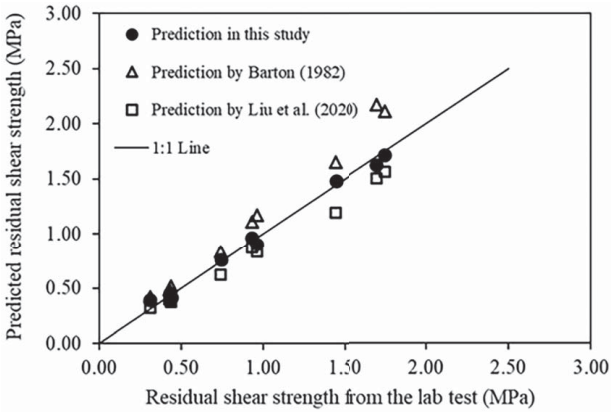


**Fig. 19.** Estimation of residual shear strength of artificial joint specimens.

**Table 7.** Comparison of the prediction of the mobilized friction angle using different models

| $\Phi$ basic | $\Phi$ mobilized | $\Phi$ mobilized (prediction by Barton 1982) and percentage difference with lab test (%) | $\Phi$ mobilized (prediction by Liu et al. 2020) and percentage difference with lab test (%) | $\Phi$ mobilized (prediction by Eq. (3) and percentage difference with lab test (%) |
|---|---|---|---|---|
| 37 | 31.85 | 37 (16.16%) | 28.23 (−11.34%) | 29.51 (−7.34%) |
| | 29.81 | 37 (24.11%) | 28.00 (−6.80%) | 29.51 (−1.00%) |
| | 31.21 | 37 (18.53%) | 27.60 (−11.56%) | 29.51 (−5.45%) |
| | 28.14 | 37 (31.47%) | 28.11 (−0.10%) | 28.95 (2.90%) |
| | 28.51 | 37 (29.78%) | 27.87 (−2.22%) | 28.95 (1.58%) |
| | 28.95 | 37 (27.82%) | 27.48 (−5.05%) | 28.95 (0.04%) |
| | 34.3 | 37 (7.89%) | 29.19 (−14.86%) | 34.09 (−0.57%) |
| | 34.01 | 37 (8.80%) | 28.95 (−14.86%) | 34.09 (0.27%) |
| | 33.83 | 37 (9.38%) | 28.54 (−15.62%) | 34.09 (0.80%) |

**Table 8.** Prediction of residual shear strength and the comparison with different models

| Data from Liu et al. (2020) | | Prediction of residual shear strength based on different models (MPa) | | | |
|---|---|---|---|---|---|
| Test | $\tau$ (MPa) Lab test | Barton's prediction and percent difference | Asadollahi's prediction and percent difference | Liu et al.'s prediction and percent difference | This study's prediction and percent difference |
| A2 | 3.11 | 2.86 (−8.04%) | 2.89 (−7.07%) | 2.69 (−13.50%) | 3.04 (−2.27%) |
| A3 | 3.14 | 3.06 (−2.55%) | 3.09 (−1.59%) | 2.8 (−10.83%) | 2.96 (−5.89%) |
| A4 | 3.10 | 3.23 (4.19%) | 3.27 (5.48%) | 2.93 (−5.48%) | 2.93 (−5.48%) |
| B2 | 2.05 | 2.4 (17.07%) | 2.42 (18.05%) | 2.1 (2.44%) | 2.1 (2.44%) |
| B3 | 1.31 | 1.52 (16.03%) | 1.55 (18.32%) | 1.38 (5.28%) | 1.38 (5.28%) |
| C3 | 3.26 | 5.01 (53.68%) | 4.73 (45.09%) | 4.02 (23.31%) | 4.05 (24.14%) |
| C4 | 3.84 | 6.46 (68.23%) | 6.11 (59.11%) | 5.19 (35.16%) | 5.32 (38.63%) |

**Table 9.** Estimation of the residual shear strength of gypsum joint specimens using equations in this study

| | | | | | | | Prediction based on formula (this study) | | |
|---|---|---|---|---|---|---|---|---|---|
| Normal stress (MPa) | $\phi_{initial}$ (degree) | UCS (MPa) | Given JRC | Actual JRC before the test | Scanned JRC after the test | Residual shear strength from Lab test (MPa) | Predicted JRC | Predicted $\phi_{mobilized}$ | Predicted residual shear strength (MPa) and percentage difference (%) |
| 0.40 | 37.50 | 4.42 | 19.60 | 16.80 | 13.64 | 0.35 | 12.49 | 26.29 | 0.33 (−6.39%) |
| 1.00 | | | | | 13.35 | 0.92 | 9.46 | 26.29 | 0.63 (−31.52%) |
| 2.00 | | | | | 16.78 | 1.64 | 5.95 | 26.29 | 1.08 (−34.15%) |

Tonon 2010). The above discussion indicated that the proposed empirical model in this study could be used to predict the residual shear strength of the jointed rock using Barton's standard profiles or randomly generated profiles. Finally, the use of Eq. (4) for estimating the residual shear strength of gypsum specimens (Le et al. 2021) was also discussed in the next section.

### Lab Test Results by Le et al. (2021)

The actual JRC value of gypsum specimens (Le et al. 2021) after the test was illustrated in Table 9. Eq. (4) was then applied to predict the residual shear strength of gypsum specimens. The result indicates that under low normal stress (0.4 MPa), Eq. (4) predicts well the residual shear strength of the gypsum specimen. The predicted residual shear strength value was 0.33 MPa, while the lab test result was 0.35 MPa (about 6.4% difference). However, under high normal stresses (1 and 2 MPa), these two equations underestimate the lab tests' results. The reason may be attributed to the small UCS of gypsum material (4.42 MPa). Under high normal stress, gypsum specimens' joint surface was severely damaged and sheared inconsistently, leading to an increase in JRC value after the test. This failure behavior of gypsum did not happen for cement specimens under high normal stress because the UCS of cement material was large (37.1 MPa). The above discussion implies that the empirical equations in this study can be used to predict the mobilized JRC, friction angle, and residual shear strength of the joint. However, the level of normal stress applied to the specimen should be considered. The ratio of the normal stress and the UCS ($\sigma$/UCS) is suggested to be smaller than 0.1, based on the analyzed data from the lab test results in this study.

## Conclusions

In this study, a series of DS tests with given JRC values (20, 19.6, and 10) were performed in both laboratory and 2D-DEM simulation. Artificial cement specimens with different JRC (20, 19.6, and 10) were cast using the PHV method and 3D-printing technology. With the specified mixing ratio of cement, sand, and water, the UCS of the cement specimens was about 37.1 MPa, classified as moderate strength based on ISRM. After replicating, the actual JRC values of artificial cement specimens were reestimated as 10, 11, and 2.4, respectively. Afterward, 2D DEM was used to simulate the mechanical behavior of rock joints under DS conditions. The joint surface in 2D DEM was modeled based on the actual scanned profile obtained from the laboratory. Barton's equation was also used to reexamine the peak shear strength of artificial joint models. Consistent results were obtained by comparing laboratory test results, numerical simulation, and Barton's shear strength equation. The following conclusions could be drawn.

1. Both lab tests and 2D DEM simulation results indicated that the peak and residual shear strength of artificial cement models (UCS = 37.1 MPa) were mainly mobilized from such a joint's friction property.
2. The shear strength and failure mechanism of artificial joint models strongly depend on the JRC, UCS, and normal stress. Cement models with high UCS (37.1 MPa) show less damaged than gypsum models (Le et al. 2021) with low UCS (4.42 MPa) based on the damage ratio analysis and observation of fracture development in 2D DEM simulation. Under the same UCS, the artificial cement specimen with a high JRC value was more damaged than that with a low JRC value. The joint surface of models under high normal stress was damaged more severely than that under low normal stress.
3. The mobilized JRC was found to be associated with the initial JRC value, UCS, and applied normal stresses. The mobilized JRC value predicted by a new equation proposed is well matched with that obtained in the laboratory and 2D DEM simulation. The mobilized friction angle was reduced from the initial basic friction value to a certain value, which was highly related to the joint's initial JRC before the test. The main reason for reduction might be attributed to the dilation behavior and decreasing contact area of the joint surface.
4. A new empirical equation was introduced to predict the joint's residual shear strength. The proposed equation could predict well the residual shear strength of artificial joint models using randomly generated profiles and Barton's standard profiles.

## Data Availability Statement

Some lab test data and simulation codes that support the findings of this study are available from the corresponding author upon reasonable request.

## Acknowledgments

This research was financially supported by the Ministry of Science and Technology, Taiwan under contract MOST 107-2625-M-008-011.

## References

Amiri, H. K., N. Babanouri, and N. S. Karimi. 2014. "The influence of asperity deformability on the mechanical behavior of rock joints." *Int. J. Rock Mech. Min. Sci.* 70: 154–161. https://doi.org/10.1016/j.ijrmms.2014.04.009.

Asadi, M. S., V. Rasouli, and G. Barla. 2013. "A laboratory shear cell used for simulation of shear strength and asperity degradation of rough rock fractures." *Rock Mech. Rock Eng.* 46 (4): 683–699. https://doi.org/10.1007/s00603-012-0322-2.

Asadollahi, P., and F. Tonon. 2010. "Constitutive model for rock fractures: Revisiting Barton's empirical model." *Eng. Geol.* 113 (1-4): 11–32. https://doi.org/10.1016/j.enggeo.2010.01.007.

Babanouri, N., and N. S. Karimi. 2015. "Modeling spatial structure of rock fracture surfaces before and after shear test: A method for estimating morphology of damaged zones." *Rock Mech. Rock Eng.* 48 (3): 1051–1065. https://doi.org/10.1007/s00603-014-0622-9.

Bahaaddini, M., P. C. Hagan, R. Mitra, and B. K. Hebblewhite. 2014. "Scale effect on the shear behaviour of rock joints based on a numerical study." *Eng. Geol.* 181: 212–223. https://doi.org/10.1016/j.enggeo.2014.07.018.

Bahaaddini, M., P. C. Hagan, R. Mitra, and M. H. Khosravi. 2016. "Experimental and numerical study of asperity degradation in the direct shear test." *Eng. Geol.* 204: 41–52. https://doi.org/10.1016/j.enggeo.2016.01.018.

Barton, N. 1973. "Review of a new shear-strength criterion for rock joints." *Eng. Geol.* 7 (4): 287–332. https://doi.org/10.1016/0013-7952(73)90013-6.

Barton, N. 1982. *Modelling rock joint behavior from in situ block tests: Implications for nuclear waste repository design*. Columbus, OH: Battelle Memorial Institute.

Cheng, C., X. Chen, and S. Zhang. 2016. "Multi-peak deformation behavior of jointed rock mass under uniaxial compression: Insight from particle flow modeling." *Eng. Geol.* 213: 25–45. https://doi.org/10.1016/j.enggeo.2016.08.010.

Deere, D. U., and R. P. Miller. 1966. *Engineering classification and index properties for intact rock*. Albuquerque, NM: Air Force Weapons Lab: Kirtland Air Base.

Fan, X., P. H. S. W. Kulatilake, and X. Chen. 2015. "Mechanical behavior of rock-like jointed blocks with multi-non-persistent joints under uniaxial loading: A particle mechanics approach." *Eng. Geol.* 190: 17–32. https://doi.org/10.1016/j.enggeo.2015.02.008.

Feder, J. 1988. *Fractals*. New York: Plenum Press.

Fei, F., and J. Choo. 2021. "Double-phase-field formulation for mixed-mode fracture in rocks." *Comput. Methods Appl. Mech. Eng.* 376: 113655. https://doi.org/10.1016/j.cma.2020.113655.

Gao, Y., Z. Liu, T. Wang, Q. Zeng, X. Li, and Z. Zhuang. 2019. "XFEM modeling for curved fracture in the anisotropic fracture toughness medium." *Comput. Mech.* 63: 869–883. https://doi.org/10.1007/s00466-018-1627-0.

Guo, S., and S. W. Qi. 2015. "Numerical study on progressive failure of hard rock samples with an unfilled undulate joint." *Eng. Geol.* 193: 173–182. https://doi.org/10.1016/j.enggeo.2015.04.023.

Jiang, M., T. Jiang, G. B. Crosta, Z. Shi, H. Chen, and N. Zhang. 2015a. "Modeling failure of jointed rock slope with two main joint sets using a novel DEM bond contact model." *Eng. Geol.* 193: 79–96. https://doi.org/10.1016/j.enggeo.2015.04.013.

Jiang, Q., X. Feng, L. Song, Y. Gong, H. Zheng, and J. Cui. 2015b. "Modeling rock specimens through 3D printing: Tentative experiments and prospects." *Acta Mech. Sin.* 32: 101–111. https://doi.org/10.1007/s10409-015-0524-4.

Krahn, J., and N. R. Morgenstern. 1979. "The ultimate frictional resistance of rock discontinuities." *Int. J. Rock Mech. Min. Sci. Geomech. Abstr.* 16 (2): 127–133. https://doi.org/10.1016/0148-9062(79)91449-9.

Le, H. K., W. C. Huang, and C. C. Chien. 2019. "Application of 3D-printing in generating artificial rock joint specimen with given JRC and its mechanical properties." In *Proc. 53rd US Rock Mechanics/Geomechanics Symp*. Alexandria, VA: American Rock Mechanics Association (ARMA).

Le, H. K., W. C. Huang, and C. C. Chien. 2021. "Exploring micromechanical behaviors of soft rock joints through physical and DEM modeling." *Bull. Eng. Geol. Environ.* 80 (3): 2433–2446. https://doi.org/10.1007/s10064-020-02087-0.

Lê, H. K., W. C. Huang, M. C. Liao, and M. C. Weng. 2018. "Spatial characteristics of rock joint profile roughness and mechanical behavior of a randomly generated rock joint." *Eng. Geol.* 245: 97–105. https://doi.org/10.1016/j.enggeo.2018.06.017.

Lee, Y. H., J. R. Carr, D. J. Barr, and C. J. Hass. 1990. "The fractal dimension as a measure of the roughness of rock discontinuity profiles." *Int. J. Rock Mech. Min. Sci. Geomech. Abstr.* 27 (6): 453–464. https://doi.org/10.1016/0148-9062(90)90998-H.

Liu, H., Z. Zhao, J. Chen, and D. Liu. 2020. "Empirical shear strength criterion for rock joints based on joint surface degradation characteristics during shearing." *Rock Mech. Rock Eng.* 53 (8): 3609–3624. https://doi.org/10.1007/s00603-020-02120-4.

Liu, Q., Y. Tian, D. Liu, and Y. Jiang. 2017. "Updates to JRC-JCS model for estimating the peak shear strength of rock joints based on quantified surface description." *Eng. Geol.* 228: 282–300. https://doi.org/10.1016/j.enggeo.2017.08.020.

Liu, Q., W. Xing, and Y. Li. 2014. "Numerical built-in method for the nonlinear JRC/JCS model in rock joint." *Sci. World J.* 2014: 735497.

Malinverno, A. 1990. "A simple method to estimate the fractal dimension of a self-affine series." *Geophys. Res. Lett.* 17 (11): 1953–1956. https://doi.org/10.1029/GL017i011p01953.

Meng, F., L. N. Y. Wong, H. Zhou, and Z. Wang. 2018. "Comparative study on dynamic shear behavior and failure mechanism of two types of granite joint." *Eng. Geol.* 245: 356–369. https://doi.org/10.1016/j.enggeo.2018.09.005.

Myers, N. O. 1962. "Characterization of surface roughness." *Wear* 5 (3): 182–189. https://doi.org/10.1016/0043-1648(62)90002-9.

Negi, A., A. K. Singh, and R. P. Yadav. 2019. "Analysis on dynamic interfacial crack impacted by SH-wave in bi-material poroelastic strip." *Compos. Struct.* 233: 111639. https://doi.org/10.1016/j.compstruct.2019.111639.

Pickering, C., and A. Aydin. 2016. "Modeling roughness of rock discontinuity surfaces: A signal analysis approach." *Rock Mech. Rock Eng.* 49 (7): 2959–2965. https://doi.org/10.1007/s00603-015-0870-3.

Sharma, P., A. K. Verma, A. Negi, M. K. Jha, and P. Gautam. 2018. "Stability assessment of jointed rock slope with different crack infillings under various thermomechanical loadings." *Arabian J. Geosci.* 11: 431. https://doi.org/10.1007/s12517-018-3772-3.

Singh, A. K., A. Negi, A. Chattopadhyay, and A. K. Verma. 2017a. "Analysis of different types of heterogeneity and induced stresses in an initially stressed irregular transversely isotropic rock medium subjected to dynamic load." *Int. J. Geomech.* 17 (8): 04017022. https://doi.org/10.1061/(ASCE)GM.1943-5622.0000891.

Singh, A. K., A. Negi, A. K. Verma, and S. Kumar. 2017b. "Analysis of stresses induced due to a moving load on irregular initially stressed heterogeneous viscoelastic rock medium." *J. Eng. Mech.* 143 (9): 04017096. https://doi.org/10.1061/(ASCE)EM.1943-7889.0001307.

Singh, A. K., A. Negi, R. P. Yadav, and A. K. Verma. 2018. "Dynamic stress concentration in pre-stressed poroelastic media due to moving punch influenced by shear wave." *J. Seismolog.* 22 (4): 1263–1274. https://doi.org/10.1007/s10950-018-9766-5.

Singh, H. K., and A. Basu. 2018. "Evaluation of existing criteria in estimating shear strength of natural rock discontinuities." *Eng. Geol.* 232: 171–181. https://doi.org/10.1016/j.enggeo.2017.11.023.

Tang, X., J. Rutqvist, M. Hu, and N. M. Rayudu. 2019. "Modeling three-dimensional fluid-driven propagation of multiple fractures using TOUGH-FEMM." *Rock Mech. Rock Eng.* 52: 611–627. https://doi.org/10.1007/s00603-018-1715-7.

Tatone, B. S. A., and G. Grasselli. 2010. "A new 2D discontinuity roughness parameter and its correlation with JRC." *Int. J. Rock Mech. Min. Sci.* 47 (8): 1391–1400. https://doi.org/10.1016/j.ijrmms.2010.06.006.

Tse, R., and D. M. Cruden. 1979. "Estimating joint roughness coefficients." *Int. J. Rock Mech. Min. Sci. Geomech. Abstr.* 16 (5): 303–307. https://doi.org/10.1016/0148-9062(79)90241-9.

Usefzadeh, A., H. Yousefzadeh, S. R. Hossein, and M. Sharifzadeh. 2013. "Empirical and mathematical formulation of the shear behavior of rock joints." *Eng. Geol.* 164: 243–252. https://doi.org/10.1016/j.enggeo.2013.07.013.

Wakabayashi, N., and I. Fukushige. 1992. "Experimental study on the relation between fractal dimension and shear strength." In *Paper for the ISRM Symp*. Lake Tahoe: Fractured and Jointed Rock Masses.

Wang, L., C. Wang, S. Khoshnevisan, Y. Ge, and Z. Sun. 2017. "Determination of two-dimensional joint roughness coefficient using support vector regression and factor analysis." *Eng. Geol.* 231: 238–251. https://doi.org/10.1016/j.enggeo.2017.09.010.